Density Functional Study of a d^2-$C_5H_5Nb(butadiene)R^+$ Ethene Polymerization Catalyst

Atte J. Sillanpää and Kari E. Laasonen*

Department of Chemistry, University of Oulu, PO Box 3000, FIN-90401 Oulun, Yliopisto, Finland

Received December 27, 2000

We have studied the ethylene polymerization catalyst $C_5H_5Nb(butadiene)Cl_2$ + MAO using primarily density functional theory (DFT). The active species was assumed to be $C_5H_5Nb(butadiene)R^+$. Chain initiation and propagation as well as different termination processes were modeled. The ethene coordination is very weak, and no free energy minimum was found. Insertion into the metal−alkyl bond has an energy barrier of 4 kcal/mol for R = CH_3 and 6 kcal/mol for R = C_2H_5. The ethene insertion transition state is clearly stabilized by agostic interaction, with metal−hydrogen distances of 2.07−2.16 Å. However, in alkyl conformations these bonds are longer and correspond to only weak agostic interaction. In the absence of strong agostic interaction the resting state alkyl complexes are floppy and different conformations interconvert easily. Termination via hydrogen transfer to a coordinated ethene molecule ejecting a terminal alkene has a high energy barrier of 17 kcal/mol. An alternative termination process via β-elimination and subsequent alkene ejection is also very expensive, 43 kcal/mol. The propagation free energy barrier for the concerted reaction is 21 kcal/mol, which consists mostly (80%) of ethene coordination. The termination free energy barrier via hydrogen transfer to coordinated alkene is 30 kcal/mol and that via β-elimination is 28 kcal/mol. The free energies have been determined in a vacuum using the harmonic approximation. The key intermediates were also optimized using MP2 supplemented with single-point calculations using CCSD. These methods gave stronger complexation energies, resulting in lowering the propagation barrier by approximately 3−4 kcal/mol and increasing the β-elimination barrier by 6−7 kcal/mol. The BSSEs in MP2 and DFT complexation energies were estimated to be 15−20 and 1−3 kcal/mol, respectively, using DZ and DVZP bases.

Introduction

Catalysis research is a very active field both in universities and in industry. Ethylene polymerization is one of the most important large-scale industry processes, where a variety of different transition metal complexes is used to produce high-quality commercial products.[1−3] One of the main goals of new catalyst design is to modify existing catalysts and to develop new ones to achieve polyethylene with a very narrow polymer size distribution. Typical modern homogeneous catalysts are of the type $L_{1-2}MX_2$ + support/promoter, where M = group III or IV transition metal, L = C_5R_5, diamine, etc., X = halogen. Both experimental and theoretical research of the mentioned catalysts has been widely reported in the literature.[1,4−17] It has been generally accepted that in these systems the active catalyst species is a neutral or cationic 14-electron d^0-metal complex of the type Cp_2MR^+.[1]

Here our research has been focused on an isoelectronic variant of the well-documented Cp_2ZrR^+ complex, Cp*Nb(2-R_1,3-R_2-butadiene)R^+, (Cp* = pentamethylcyclopentadienyl), which has been reported to produce polyethylene with a very narrow polymer size distribution (M_w/M_n = 1.05).[18,19] To our knowledge the mechanism has not been previously studied computationally.

(1) Brintzinger, H. H.; Fischer, D.; Müllhaupt, R.; Rieger, B.; Waymouth, R. M. *Angew. Chem., Int. Ed. Engl.* **1995**, *34*, 1143.
(2) Allen, G. *Comprehensive Polymer Science*, 1st ed.; Pergamon Press: Oxford, 1989; Vol. 4.
(3) McKnight, A. L.; Waymouth, R. M. *Chem. Rev.* **1998**, *98*, 2587−2598.
(4) Thorshaug, K.; Stövneng, J. A.; Rytter, E.; Ystenes, M. *Macromolecules* **1998**, *31*, 7149−7165.
(5) Petitjean, L.; Pattou, D.; Ruiz-Lopez, M. F. *J. Phys. Chem.* **1999**, *103*, 27−35.
(6) Grubbs, R.; Coates, G. *Acc. Chem. Res.* **1996**, *29*, 85−93.
(7) Das, P. K.; Dockter, D. W.; Fahey, D. R.; Lauffer, D. E.; Hawkins, G. D.; Li, J.; Zhu, T.; Cramer, C. J.; Truhlar, D. G.; Dapprich, S.; Froese, R. D. J.; Holthausen, M. C.; liu, Z.; Mogi, K.; Vyboishchikov, S.; Musaev, F. G.; Morokuma, K. *Ethylene Polymerization by Zirconocene Catalysis*; Supercomputing Institute Research, 1998.
(8) Lohrenz, C. W.; Woo, T. K.; Ziegler, T. *J. Am. Chem. Soc.* **1995**, *117*, 12793−12800.
(9) Froese, R. D. J.; Musaev, D. G.; Matsubara, T.; Morokuma, K. *J. Am. Chem. Soc.* **1997**, *119*, 7190−7196.
(10) Bierwagen, E. P.; Bercaw, J. E.; Goddard, W. A. *J. Am. Chem. Soc.* **1994**, *116*, 1481−1489.
(11) Kawamura-Kuribayashi, H.; Koga, N.; Morokuma, K. *J. Am. Chem. Soc.* **1992**, *114*, 8687−8694.
(12) Woo, T. K.; Margl, P. M.; Lohrenz, J. C. W.; Blöchl, P. E.; Ziegler, T. *J. Am. Chem. Soc.* **1996**, *118*, 13021−13030.
(13) Margl, P.; Deng, L.; Ziegler, T. *J. Am. Chem. Soc.* **1999**, *121*, 154−162.
(14) Margl, P.; Deng, L.; Ziegler, T. *Organometallics* **1998**, *17*, 933−946.
(15) Margl, P.; Deng, L.; Ziegler, T. *J. Am. Chem. Soc.* **1998**, *120*, 5517−5525.
(16) Margl, P. M.; Woo, T. K.; Ziegler, T. *Organometallics* **1998**, *17*, 4997−5002.
(17) Margl, P.; Lohrenz, J. C.; Ziegler, T.; Blöchl, P. E. *J. Am. Chem. Soc* **1996**, *118*, 4434−4441.
(18) Mashima, K.; Fujikawa, S.; Tanaka, Y.; Urata, H.; Oshiki, T.; Tanaka, E.; Nakamura, A. *Organometallics* **1995**, *14*, 2633−2640.

10.1021/om0010924 CCC: $20.00
Publication on Web 03/06/2001

In contrast to the Zr analogue and the majority of early transition metal catalysts, the active species is a formally d^2-cationic metal complex. The original concept behind the preparation of the niobium catalysts was the equal electron count with respect to the parent $Cp_2MR^{(+/0)}$ 14-electron catalysts. Our goal is to determine the polymerization mechanism and compare the similarities and differences with other 14-electron catalysts.

Computational Details

The results and energies presented here have been computed with the Gaussian98 package,[20] unless noted otherwise. Dmol[3] and Finger[21−23] were also used to scan the potential energy surfaces, some preliminary optimizations, and the reference. We also performed a few Car−Parrinello[24] molecular dynamics (CPMD) runs using the Finger code. In these calculations the plane wave basis with an kinetic energy cutoff of 30 Ry was used. The MD time step was 0.16 fs. Most Gaussian98 calculations were performed with the double-ζ quality LanL2DZ (basis B1) basis set, which uses an effective core potential, corrected for scalar relativistic effects replacing 28 electrons on niobium,[25−27] and the Dunning/Huzinaga full double-ζ on the other atoms.[28] Several geometries were also calculated with a slightly improved basis (basis B2): for all nonmetal atoms we chose the Dunning/Huzinaga double-ζ valence basis set D95V,[28] where for methyl, ethyl, and ethene moieties, diffuse and polarization functions were added (++(d,p)), and for niobium we used the LanL2DZ basis. The backbone (cyclopentadienyl and butadiene) geometries varied only slightly in the course of the reaction, which in part justifies the classification of the complex into an active part and spectator ligands. This scheme has been previously utilized in similar calculations.[9,11,29−31] Basis sets of this and lower level (on the active part) have been successfully applied to study analogous catalytic processes on Zr-systems.[5,9,30] The third basis (B3) is the same as B2 augmented with a set of f-type Gaussians with an exponent $\alpha = 0.952$[32] on niobium.

Transition states were located by first performing a potential energy surface scan between previously determined local minima corresponding to possible resting states, followed by either synchronous transit-guided quasi-Newton (STQN) or Berny optimization implemented in Gaussian98 to find the actual transition state. Local minimum and transition state DFT structures have been verified with frequency calculations. Frequency calculations were not performed for MP2-optimized structures, as they were similar to the DFT ones. With Finger the transition states were not confirmed by frequency analysis, but optimization was considered complete when the forces were negligible. No symmetry constraints were used in reported structures. Thermodynamical data were extracted from frequency calculations assuming harmonic approximation at 298.15 K and treating $3N - 6$ degrees of freedom explicitly as vibrations without scaling. With large and soft molecules this may cause significant error.[16]

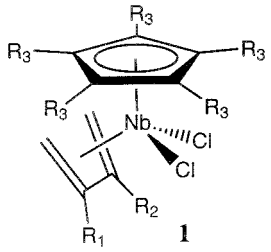

1

Figure 1. $R_i = H, CH_3$.

Computational Method

There are some short-hand notations used in this paper. The energies are labeled as follows: A/B//C/D, where A stands for the method used for the energy calculation (BP86 if omitted), B for the basis set in the energy calculation (B1 if omitted), C for the method used in the geometry optimization (the same as A if omitted), and D for the optimization basis (the same as B if omitted). The geometries are denoted by alphanumerals, where the number gives the overall geometry, the number of carbon atoms in the growing polymer chain is given by the letter (**a** = CH_3, **b** = C_2H_5 ...), and **alpha** and **beta** refer to α- and β-agostic geometry of the polymer chain, respectively (see Figure 3). Electronic energies do not include zero-point energy and have not been corrected for BSSE unless stated otherwise. BP86/B1 energies have been used for the figures.

In DFT calculations we used the Becke-88 exchange functional[33] and Lee−Yang−Parr[34] or Perdew[35,36] correlation functionals (BLYP and BP86, respectively) and B3LYP.[37] We performed also ab initio calculations (HF, MP2,[38] and CCSD(T)[39]) in BP86 optimized and in self-consistent geometries, for calibration and reference. Because of the formal d-population of the model complex and possibility of nondynamical correlation effects due to near degeneracies, we used the most sophisticated method we could afford (CCSD). The coupled-cluster calculations were performed by freezing the carbon and nitrogen 1s core states. The HOMO−LUMO gap was calculated to be 1.5−2.6 eV (DFT) and 7.5−12 eV (all ab initio calculations), depending on the complex enabling the restricted spin approximation, which was used in all calculations. Some complexes were also tested for triplet state, but they were invariably higher in energy than the singlet state.

Different computational approaches were briefly compared by calculations of similar complexes. Margl et al. calculated the ethene coordination to $NH(CH_2)_2NHNbCH_2CH_3$ to be exothermic by −54.3 kcal/mol (BP86/TVZP/DVZ)[14] with ADF,

(19) Mashima, K.; Fujikawa, S.; Urata, H.; Tanaka, E.; Nakamura, A. *J. Chem. Soc., Chem. Commun.* **1994**, 1623−1624.
(20) Frisch, M. J.; Trucks, G. W.; Schlegel, H. B.; Scuseria, G. E.; Robb, M. A.; Cheeseman, J. R.; Zakrzewski, V. G.; Montgomery, J. A.; Stratmann, R. E.; Burant, J. C.; Dapprich, S.; Millam, J. M.; Daniels, A. D.; Kudin, K. N.; Strain, M. C.; Farkas, O.; Tomasi, J.; Barone, V.; Cossi, M.; Cammi, R.; Mennucci, B.; Pomelli, C.; Adamo, C.; Clifford, S.; Ochterski, J.; Petersson, G. A.; Ayala, P. Y.; Cui, Q.; Morokuma, K.; Malick, D. K.; Rabuck, A. D.; Raghavachari, K.; Foresman, J. B.; Cioslowski, J.; Ortiz, J. V.; Stefanov, B. B.; Liu, G.; Liashenko, A.; Piskorz, P.; Komaromi, I.; Gomperts, R.; Martin, R. L.; Fox, D. J.; Keith, T.; Al-Laham, M. A.; Peng, C. Y.; Nanayakkara, A.; Gonzalez, C.; Challacombe, M.; Gill, P. M. W.; Johnson, B. G.; Chen, W.; Wong, M. W.; Andres, J. L.; Head-Gordon, M.; Replogle, E. S.; and Pople, J. A. *Gaussian 98*; Revision A.6 ed.; Gaussian Inc.: Pittsburgh, PA, 1998.
(21) Finger is a plane wave based pseudopotential density functional code developed mainly in the Helsinki University of Technology. This code is also capable of doing the Car−Parrinello molecular dynamics.
(22) Laasonen, K.; Pasquarello, A.; Car, R.; Lee, C.; Vanderbilt, D. *Phys. Rev. B* **1993**, *47*, 10142−10153.
(23) Sprik, M.; Hutter, J.; Parrinello, M. *J. Chem. Phys.* **1996**, *105*, 1142−1152.
(24) Car, R.; Parrinello, M. *Phys. Rev. Lett.* **1985**, *55*, 2471.
(25) Hay, P. J.; Wadt, W. T. *J. Chem. Phys* **1985**, *82*, 299.
(26) Hay, P. J.; Wadt, W. T. *J. Chem. Phys.* **1985**, *82*, 270.
(27) Wadt, W. T.; Hay, P. J. *J. Chem. Phys.* **1985**, *82*, 284.
(28) Dunning, T. H., Jr.; Hay, P. J. *Modern Theoretical Chemistry*; Plenum: New York, 1976.
(29) Koga, N. *Theor. Chem. Acc.* **1999**, *102*, 285−292.
(30) Musaev, D. M.; Froese, R. D. J.; Svensson, M.; Morokuma, K. *J. Am. Chem. Soc.* **1997**, *119*, 367−374.
(31) Camanyes, S.; Maseras, F.; Moreno, M.; Lledos, A.; Lluch, J. M.; Bertran, J. *J. Am. Chem. Soc.* **1996**, *118*, 4617−4621.
(32) Ehlers, A. W.; Böhme, M.; Dapprich, S.; Gobbi, A.; Höllwarth, A.; Jonas, V.; Köhler, K. F.; Stegmann, R.; Veldkamp, A.; Frenking, G. *Chem. Phys. Lett.* **1993**, *208*, 111−114.
(33) Becke, A. D. *Phys. Rev. A* **1988**, *38*, 3098.
(34) Lee, C.; Yang, W.; Parr, R. G. *Phys. Rev. B* **1988**, *37*, 785.
(35) Perdew, J. P.; Zunger, A. *Phys. Rev. B* **1981**, *23*, 5048.
(36) Perdew, J. P. *Phys. Rev. B* **1986**, *33*, 8822−8824.
(37) Becke, A. D. *J. Chem. Phys.* **1993**, *98*, 5648−5652.
(38) Moller, C.; Plesset, M. S. *Phys. Rev.* **1934**, *46*, 618.
(39) Pople, J. A.; Head-Gordon, M.; Raghavachari, K. *J. Chem. Phys.* **1987**, *87*, 5968.

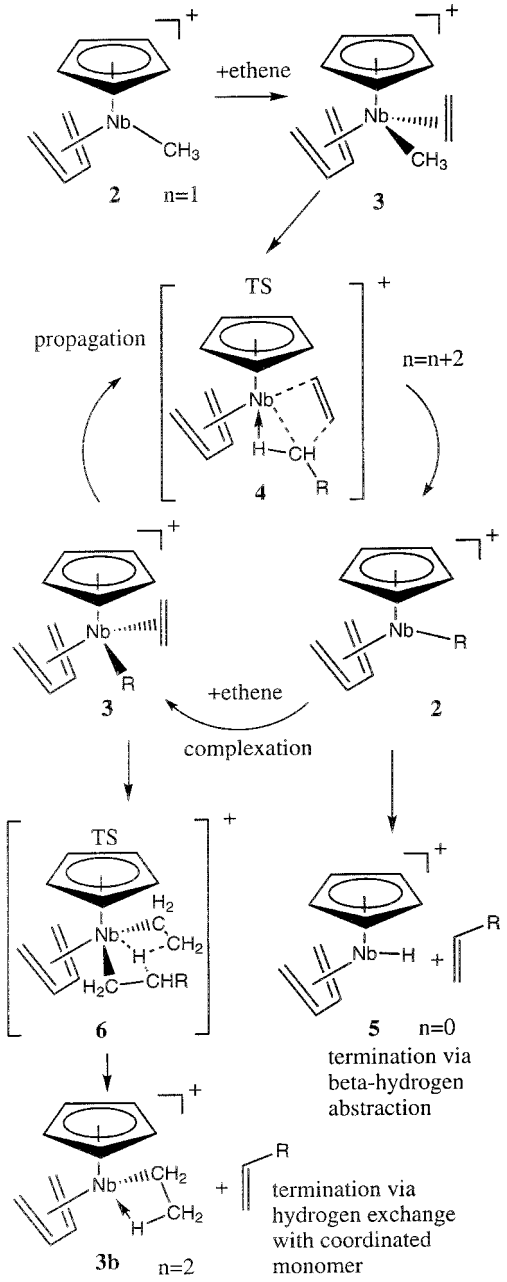

Figure 2. Catalytic cycle with propagation, initiation, and termination. In the name of the structure the number in boldface denotes the general structure, i.e., **2** for alkyl complex, the letter denotes the number of carbon atoms in the growing polymer chain as **a** = 1 = CH_3, **b** = 2 = C_2H_5, etc., and **alpha** and **beta** denote the α- and β-agostic orientation of the polymer chain. Square brackets indicate transition state structure.

while we found −39.7 kcal/mol (BLYP/DNP) with the MSI-code Dmol[3]. More complexation energies are presented in Table 1 using different levels of theory and basis sets. The DFT coordination energies are in a range of 10 kcal/mol, and the major difference comes from the used functional. The effect of including the noniterative triples correction to the CCSD energy is small. For further comparison we recalculated the ethene coordination to $Cp_2ZrC_2H_5^+$ (front side) to be exothermic by −8.3 (BLYP/B2), −11 (BP86/B1), and −23.1 kcal/mol (MP2/B1//BP86). The theoretical DFT results in the literature are in the range −6 to −9.5 kcal/mol.[4,5,7,8]

The key intermediates on the polymerization cycle were also calculated using the different methods; see Table 2. We report the following results to validate the use of single reference

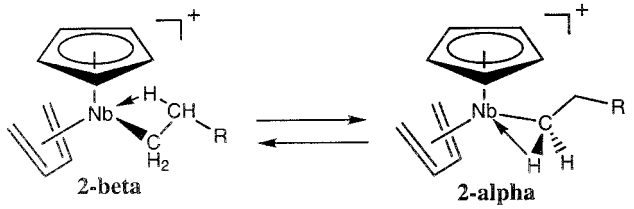

Figure 3. β- and α-agostic alkyl conformations. In **2b-alpha** the H_α atoms are equivalent, but the other arrow designating weak agostic interaction is omitted for clarity.

Table 1. Ethene Coordination Energies in kcal/mol to $NH(CH_2)_2NHNbCH_2CH_3$ Complex[a]

	Basis		
method	B1	B2	B3
BLYP	−41.0	−40.7	−41.5
BP86	−50.0	−50.2	−49.5
B3LYP	−42.8	−44.0	
MP2	−56.7		−62.9
CCSD	−38.9		−44.9
CCSD(T)	−39.9		

[a] Basis sets (B1, B2, and B3) have been described in the text. Geometries have been determined either at the B1 or B2 level. The CCSD-calculations used BP86/B2 geometries.

Table 2. Energies of the Key Intermediates of the Ethene Insertion to Ethyl Complex Calculated with Various Levels of Theory[a]

	3b-alpha1/2[b]	**[4b]**[b]	**[4b]** $\Delta E^{\ddagger}$[c]	**5**+ethene[d]
BLYP/B1	7.4(9.8)	11.8(14.8)	4.3(5.0)	37.4
BLYP/B2	7.4	10.8	3.5	37.4
BLYP/B3//B2	7.8(9.1)	11.0(12.9)	3.2(2.1)	37.6
BP86/B1	3.6(5.5)	5.6(8.4)	1.3(2.1)	45.5(42.4)[f]
BP86/B3//B1	4.6(5.8)	5.3(7.1)	0.7(1.3)	45.1(39.5)[f]
HF	5.1	21.0	15.9	34.6
MP2	−10.1(4.6)	−7.4(12.2)	2.5(7.6)	56.5
MP2/SDD[e]	−7.7	−6.7	0.9	53.7
MP2//BP86	−9.8	−7.9	2.0	57.3
MP2/B3//B1	−14.0(0.7)	−13.9(4.2)	0.1(3.5)	65.7(49.1)[f]
CCSD//MP2	−2.3	3.4	5.7	46.4
CCSD(T)//MP2				48.8
CCSD/B3//MP2				53.6

[a] Energies are reported in kcal/mol and the BSSE-corrected energies, where available, are given in parentheses. The alpha-numerics are explained, e.g., in Figure 2. [b] Energies relative to ethyl alkyl complex **2b-beta** and free ethene. [c] Energies relative to lower energy α-agostic ethyl η^2-ethene complex **3b-alpha1/2**, i.e., the insertion barrier after ethene complexation. [d] β-Elimination product energies relative to **2b-beta**. [e] The Stuttgart/Dresden basis and relativistic effective core potential for Nb and Dunning/Huzinaga full double-ζ for other atoms; SDD keyword in Gaussian98. [f] The fractioning of the **2b-beta** complex for the BSSE calculations is not straightforward, as it divides the alkyl group in two, but tentative values are given as the correction is unavoidable for MP2.

methods and the lack of important nondynamical correlation effects. According to the coupled-cluster theory, the largest single excitation cluster amplitudes are in the range 0.04−0.07 (the largest being 0.08 for ethene), and T1 diagnostic values for these complexes are below the suggested threshold of 0.02.[40]

The MP2/B3//B1 ethene complexation energy to the ethyl complex **2b-beta** was 19.2 kcal/mol higher than according to BP86/B3//B1 (see Table 2.). This seems to be a trend in organometallic complexation energies.[41−45] The large difference is only in the complexation, as the relative energies of the complexed species do not change so dramatically (note that

(40) Lee, T. J.; Taylor, P. R. *Int. J. Quantum Chem. Symp.* **1989**, *11*, 199.

we consider an alkyl complex here as an alkene complexed to a metal hydride). CCSD/B3//MP2/B1 calculations on the β-elimination reaction components revealed 7 kcal/mol more correlation energy in the ethyl complex **2b-beta** relative to **8**. This means, not surprisingly, that the smallest basis (B1) is clearly inadequate for CCSD, while even the DZ description reveals stronger complexation than found with the other methods. These results will be considered in the discussion at the end of the paper. The differences in Tables 1 and 2 energies are, in addition to BSSE, see below, probably due to the extent of (dynamical) correlation recovered in the calculations. However, this will not change the mechanistic paths, but merely affects the relative probabilities between the bimolecular (β-elimination termination and complexation) and unimolecular (reactions involving complexed monomer) steps.

Improving the basis has relatively little effect on the relative energies in the DFT calculations, as can be seen in Tables 1 and 2. We therefore excluded the f-functions in DFT calculations due to small changes in geometries (bonds average(BP86/B3−BP86/B1) = −0.002 Å, rms = 0.009) to decrease the computational load. The effect of f-polarization functions on the transition metal centers in organometallic compounds has been considered unimportant also in other DFT studies,[46−48] while their effect is crucial in the correlated ab initio methods.

Basis set superposition error (BSSE) effects were studied by calculating the counterpoise corrections ("7-point" BSSE correction formula[49]). From Tables 1 and 2 can be seen that MP2 complexation energies are much larger than any others unless they are corrected for BSSE. The DFT methods and MP2 display BSSEs of 1−3 and 15−20 kcal/mol, respectively. The BSSE diminishes after addition of polarization and diffuse functions, but the DFT energies do not change substantially and are, probably, due to cancellation of errors, close to the uncorrected values obtained with the smallest basis (B1). The insertion barrier **[4b]** was also calculated with Finger, a BSSE-free plane wave code, yielding $\Delta E^{\ddagger}$ = 12.3 (BLYP) and 3.6 (BP86) kcal/mol. The large BSSE in the MP2 results, relative to DFT, is due to configuration set superposition error (CSSE), as proposed by Duijneveldt et al.[45,50] According to van Duijneveldt et al. the magnitude of CSSE should rapidly decrease when more electron correlation is recovered using higher correlated methods. However, due to the modest basis sets used in the CCSD calculations, it is indecisive to estimate the amount of BSSE or CSSE in those energies. The CCSD calculations are the best we could afford, and we take those as a guide for rough calibration; that is, the complexation is underestimated by the other methods.

According to the level of theory the bond lengths decrease as follows, MP2 < BP86 < BLYP, although the changes are small and the general geometries of the potential energy extrema are similar. Similarly the complexation energies increase in the opposite order. The largest differences are in the Nb−$H_{agostic}$ bonds. The rms bond length deviation between BP86 and MP2 was 0.019 (and 0.013 with Nb−H bonds removed).

As there is some variance in energetic and structural results between the two density functionals, we used both BLYP and BP86 to diminish the possibility of functional artifacts. The results with all methods seem to converge well, apart from the complexation energy. This holds especially for HF and (uncorrected) MP2, but the *relative* energies of the complexed species agree with all methods, excluding HF (compare the $\Delta E^{\ddagger}$ in Table 2).

We believe that BP86 gives qualitatively correct results with a significantly reduced computational cost. This is important, as one of our objectives is also to find a method that is not so computationally expensive that it can be applied to real catalysts containing many more atoms than present in the model complex of this study. Another point in favor of DFT is the small BSSE, which cannot be neglected in MP2 calculations.[51,52] Therefore, DFT is better suited for determination of the full potential energy surface (PES), as the partitioning of the supermolecule to perform the counterpoise calculations becomes an ill-defined mathematical problem[49] (e.g., in the backward direction the correction is generally different). Further, the use of DFT enables us to supplement the static calculations with CPMD simulations. Previously DFT (especially BP86) has been reported to give dissociation energies within 5 kcal/mol of the experimental values in organometallic systems.[42,53−55] Our test calculations fall in this range according to the intramolecular barriers, but show a slightly larger variance in the intermolecular energy differences.

Results

The Catalytic System. The [η^5-$C_5(R_3)_5$(η^4-*cis*-2-R_1,3-R_2-butadiene)$NbCl_2$ system (see Figure 1) has been synthesized and experimentally studied by Mashima et al.[18,19,56−58] They have reported this type of catalysts to produce polyethylene with very narrow polydispersity (M_w/M_n = 1.05). We have studied the mechanism in order to understand the interesting performance.

In the system of our interest the active catalyst is prepared in situ by adding a suitable promoter, e.g., methylaluminoxane (MAO), into a toluene solution of the dichloride precursor (**1**). MAO is first believed to replace one chloride ligand with a methyl group and then to remove the other chloride ligand. The resulting cationic 14-electron alkyl complex is widely accepted to be the active species in this type of polymerization catalysts.[1,6,10] Specifically, Mashima et al. reported this cationic alkyl species as the activated complex responsible for polymerization activity.[18,19,59] They also reported notable ligand substituent effects on the polymer size distribution and catalyst stability.[18] However, to first find out the most essential electronic effects, we have concentrated in a model system, where $R_1 = R_2 = R_3 = H$ (see Figure 1). The most narrow polymer size distribution was experimentally achieved by using $R_3 = CH_3$, e.g., Cp* (pentamethylcyclopentadienyl, $C_5(CH_3)_5$). The Cp catalyst system ($R_3 = H$, $R_1 = R_2 = CH_3$)

(41) Weiss, H.; Ehrig, M.; Alrichs, R. *J. Am. Chem. Soc.* **1994**, *116*, 4919−4928.
(42) Li, J.; Schreckenbach, G.; Ziegler, T. *J. Phys. Chem.* **1994**, *98*, 4838−4841.
(43) Dapprich, S.; Pidun, U.; Ehlers, A. W.; G., F. *Chem. Phys. Lett.* **1995**, *242*, 521−526.
(44) Ehlers, A. W.; Frenking, G. *J. Am. Chem. Soc.* **1994**, *116*, 1514−1520.
(45) Zaric, S.; Hall, M. B. *J. Phys. Chem.* **1997**, *101*, 4646−4652.
(46) Landis, A. R.; Hilfenhaus, P.; Feldgus, S. *J. Am. Chem. Soc.* **1999**, *121*, 1, 8741−8754.
(47) Rosa, A.; Ehlers, A. W.; Baerends, E. J.; Snijders, J. G.; te Velde, G. *J. Phys. Chem.* **1996**, *100*, 5690−5696.
(48) Choi, S.-H.; Lin, Z. *Organometallics* **1999**, *18*, 2473−2478.
(49) Lendway, G.; Mayer, I. *Chem. Phys. Lett.* **1998**, *297*, 365−373.
(50) van Duijneveldt, F. B.; van de Rijdt, J. G. C. M.; van Lenthe, J. H. *Chem. Rev.* **1994**, *94*, 1873−1885.
(51) Tasi, G.; Mizukami, F.; Toba, M.; Niwa, S.; Palinko, I. *J. Phys. Chem.* **2000**, *104*, 1337−1345.
(52) Barnes, L. A.; Liu, B.; Lindh, R. *J. Chem. Phys.* **1993**, *98*, 3978−89.
(53) Li, J.; Schreckenbach, G.; Ziegler, T. *J. Am. Chem. Soc.* **1995**, *117*, 486-494.
(54) Folga, E.; Ziegler, T. *J. Am. Chem. Soc.* **1993**, *115*, 5169−5176.
(55) Martell, J. M.; Goddard, J. D.; Eriksson, L. A. *J. Phys. Chem.* **1997**, *101*, 1927−1934.
(56) Mashima, K.; Nakayama, Y.; Kaidzu, M.; Ikushima, N.; Nakamura, A. *J. Organomet. Chem.* **1998**, *557*, 3−12.
(57) Mashima, K.; Kaidzu, M.; Nakayama, Y.; Nakamura, A. *Organometallics* **1997**, *16*, 1345−1348.
(58) Okamoto, T.; Yasuda, H.; Nakamura, A.; Yasushi, K.; Kanehisa, N.; Nobutami, K. *J. Am. Chem. Soc.* **1988**, *110*, 5008−5017.
(59) Mashima, K.; Fujikawa, A.; Nakamura, A. *J. Am. Chem. Soc* **1993**, *115*, 10990−10991.

also displayed catalytic activity, but the polymer had low monodispersity ($M_w/M_n = 4.4$).[59]

We have not modeled MAO computationally. We have assumed that MAO does not have direct influence on the metal center, but only stabilizes the cation as a weakly coordinating counterion.[4] We have not taken solvent effects into account in the computed energies, as toluene is a rather inert solvent and the gas phase assumption is expected to give a qualitatively correct explanation of the intrinsic electronic phenomena of the reactions.

General Mechanism. For the ethene polymerization with neutral group III and cationic group IV complexes, which are isoelectronic to **2** (see Figure 2), two principal mechanisms have been considered: Cosseé−Arlman[60−62] and Green−Rooney.[63,64] Other mechanisms, such as Brookhart−Green,[65] can be thought of as variants of these two. For example, α-agostic interaction may be considered as an intermediate between an alkyl hydrogen and a metal hydride and may occur at different stages in the catalytic cycle.

1. Cosseé−Arlman. Ethene coordinates to the vacant metal site in η^2-fashion, followed by 1,2-insertion to the alkyl−metal bond via a four-center transition state structure. Insertion produces a new vacant site for the next monomer.

2. Green−Rooney. The alkyl complex undergoes an α-hydrogen abstraction to produce a hydride−alkylidene complex. Ethene monomer then coordinates in η^2-fashion and subsequently forms a metallacyclobutane. Hydride migration to the C_α reproduces the initial alkyl geometry with a polymer chain extended with one monomer.

Mechanisms similar to 1 have been proposed, for example, for a d^0-Cp_2ZrR^+ system[5,6] and several other d^0-catalyst systems.[15] Mechanism 2 requires d-electrons on the metal to make formal oxidative addition possible and has been proposed, for example, for a Ta complex[66] and Cp_2*NbC_2H_5.[67] Due to the similarities of Ta and Nb chemistry and because alkylidene[57,68] intermediates and hydrides for Nb have been reported, we considered mechanism 2 as a viable alternative.

Polymerization Reaction. The schematic reaction cycle is presented in Figure 2, including the key intermediates of initiation, propagation, and possible termination steps. The reaction cycle has been divided into subsections, where each step is studied in detail, according to the intermediates on the reaction path. In the next section the methyl complex, resulting from the catalyst precursor activation, is treated together with other alkyl intermediates, followed by alkyl η^2-ethene complexes **3**. Finally the insertion transition states **[4]**, alkylidene complexes, and different termination mechanisms are discussed.

Table 3. Energies of Representative Geometries on the Catalytic Cycle[d]

		BP86/B1		BLYP/B2	
structure	energy relative to	Δ*E*	Δ*G*	Δ*E*	Δ*G*
3a	**2a**+ethene	−1.0	13.7	4.2	18.4
2b-alpha	**2b-beta**	2.3	0.4	0.4	−1.0
2c-alpha	**2a**+ethene	−24.3	−9.1	−20.6	−5.1
2c-beta	**2a**+ethene	−27.3	−11.0	−21.5	−5.8
2d-beta	**2b-beta**+ethene	−25.2	−10.5	−21.2	−6.5
3b-alpha1	**2b-beta**+ethene	3.7	16.6		
3b-alpha2	**2b-beta**+ethene	4.2	18.1	7.4	21.0
3b-beta	**2b-beta**+ethene	4.3	19.1	8.7	23.7
[4a]	**2a**+ethene	3.6	20.7	11.4	27.4
[4b]	**2b-beta**+ethene	5.6	21.3	10.8	26.7
5 (+ethene)	**2b-beta**	45.6	29.6	37.4	22.0
5 (+propene)	**2c-beta**	42.0	25.8	33.1	17.6
5 (+butene)	**2d-beta**	43.1	27.1	33.7	18.0
[β-elim. TS][b]	**2c-beta**	*a*	≈28	*a*	21.4
[6b]	**2b-beta**+ethene	16.5	30.1	22.2	36.5
[7b]	**2b-beta**	33.2	28.3	25.1[c]	22.8[c]
8b	**2b-beta**	21.6	20.5		
9d	**2b-beta**+ethene	−12.2	1.4		
[10d]	**9d**	24.9	26.0		
11d	**2b-beta**+ethene	−10.4	5.8		
[12d]	**11d**	23.1	22.7		
13d	**2b-beta**+ethene	−25.5	−10.1		

[a] Potential energy maximum is at infinite separation. [b] Propyl chain as the model for polymer, where the Nb−C_α distance is 2.76 Å for BP86 and 2.69 for BLYP. [c] Results calculated with B1 basis. [d] Energies are reported in kcal/mol relative to a suitable species (given in the second column).

Alkyl Resting State. Catalyst activation results in the alkyl complex **2a**. The geometric data of different alkyl species are shown in Table 4 and thermodynamic data in Table 3. The butadiene moiety has been previously shown to prefer supine orientation, and therefore we did not consider the prone rotamers. (The supine (exo) coordination mode has been drawn in the Figures. The prone (endo) configuration results after 180° rotation of the butadiene center−Nb axis.)[69,70] A methyl group occupying the place of the growing polymer after activation is capable of only α-agostic bonding due to lack of β-hydrogens. Bonding between H_α and Nb in methyl through propyl alkyl complexes is, however, very weak. Nevertheless, **2b,c-alpha** were found only less than 3 kcal/mol ($\Delta G < 1$) above β-agostic conformers. β-Agostic bonding in complexes **2b,c,d-beta** is moderate. Typical agostic Nb−H_β bond lengths were between 2.21−2.25 Å (BP86) and 2.25−2.40 Å (BLYP). Zr−H distances in analogous complexes are on the order of 2.05−2.15 Å.[8] All β-agostic structures are similar at the metal center, and it is therefore justified to use an ethyl group as a model of the growing polymer chain. Attempts to locate minima corresponding to γ-agostic alkyl structures were unsuccessful.

The fluxionality of the propyl chain was studied by scanning the potential energy surface corresponding to the rotation around the Nb−C_α−C_β−H_β torsion. The minimum structures correspond to **5c-beta**, only the hydrogen being responsible for the agostic bond changes. The low interconversion barrier of 1.8 kcal/mol (BLYP/B2), weak agostic interactions, and the small energy difference between different isomers imply that the propyl chain is very floppy. In a Car−Parrinello molec-

(60) Arlman, E. J. *J. Catal.* **1964**, *3*, 89−98.
(61) Arlman, E. J.; Cossee, P. *J. Catal.* **1964**, *3*, 99−104.
(62) Cossee, P. *J. Catal.* **1964**, *3*, 80−88.
(63) Ivin, K. J.; Rooney, J. J.; Stewart, C. D.; Green, M. L. H.; Mahtab, R. *J. Chem. Soc., Chem. Commun.* **1987**, 1410−1411.
(64) Green, M. L. H. *Pure. Appl. Chem.* **1978**, *50*, 27−35.
(65) Brookhart, M.; Green, M. L. H. *J. Organomet. Chem.* **1983**, *250*, 395−408.
(66) Turner, H. W.; Schrochk, R. R. *J. Am. Chem. Soc.* **1982**, *104*, 2331−2333.
(67) Doherty, N. M.; Bercaw, J. E. *J. Am. Chem. Soc.* **1985**, *107*, 2670−2682.
(68) Mashima, K.; Matsuo, Y.; Tani, K. *Organometallics* **1999**, *18*, 1471−1481.
(69) Yasuda, H.; Tatsumi, K.; Okamoto, T.; Mashima, K.; Lee, K.; Nakamura, A. *J. Am. Chem. Soc.* **1985**, *107*, 2410−2422.
(70) Yasuda, H.; Nakamura, A. *Angew. Chem.* **1987**, *99*, 745−764.

Table 4. Geometrical Data[j]

property	2a[e]	2b-beta	2c-beta	2d-beta	2b-alpha[e]	2c-alpha	3a	3b-alpha1	3b-alpha2	3b-beta	[4a]	[4b]	5	[6b]	[7b]	8b	9d	[10d]	11d	[12d]	13d
Cp−Nb	2.138	2.135	2.136	2.136	2.132	2.133	2.154	2.159	2.163	2.152	2.149	2.150	2.123	2.150	2.137	2.117	2.143	2.164	2.154	2.174	2.135
C1−Nb	2.216	2.227	2.226	2.225	2.228	2.233	2.474	2.263	2.383	2.381	2.297	2.306	2.194	2.370	2.424	2.651[i]	4.057[i]	2.434[i]	2.856[i]	2.431[i]	2.285[a]
C2−Nb	2.425	2.427	2.426	2.424	2.434	2.432	2.533	2.441	2.503	2.516	2.436	2.443	2.409	2.462	2.462	2.362	3.377	2.455	2.471	2.394	2.459
C3−Nb	2.425	2.442	2.443	2.449	2.434	2.435	2.477	2.474	2.499	2.510	2.454	2.456	2.409	2.459	2.525	2.436	2.573	2.462	2.471	2.438	2.449
C4−Nb	2.216	2.274	2.274	2.283	2.228	2.227	2.289	2.297	2.305	2.304	2.340	2.337	2.194	2.370	2.485	2.349	2.182	2.340	2.383	2.382	2.247
Bd−Nb	1.900	1.936	1.935	1.940	1.912	1.914	2.090	1.986	2.063	2.073	2.015	2.021	1.877	2.061	2.083	2.054	2.820	2.056	2.193	2.047	1.957
C_α−Nb	2.117	2.145	2.149	2.152	2.104	2.104	2.227	2.165	2.191	2.265	2.259	2.273		2.534,2.524	1.944	2.000	2.107	2.136[b]	2.167[b]	2.270[b]	2.615[b]
C_β−Nb		2.629	2.656	2.636	3.394	3.410		3.366	3.411	2.689		3.595		2.668[a],2.672	3.366	3.149	2.416	2.432	2.429	2.547	2.165
C_γ-Nb			3.852	3.870		4.193											2.145	2.287	2.139	2.217	2.973
C_{up}−Nb							2.425	2.890	2.542	2.650	2.388[f]	2.412[f]									
C_{down}−Nb							2.619	3.092	2.726	2.797	2.621[g]	2.608[g]									
H_α−Nb	2.591[e]	2.620	2.614	2.619	2.434[e]	2.314,2.521	2.690	2.205	2.249	2.876	2.163	2.067	1.762[d]	3.002−3.067	1.772[c],2.198	2.775		1.891[c]	2.862[c]	1.921[c]	2.213
H_α−C_α	1.119[e]	1.113	1.115	1.113	1.132[e]	1.144	1.112	1.154	1.150	1.098	1.145	1.159		1.092	1.157	1.103	1.107	1.101	1.098	1.100	1.150
H_β−Nb		2.247	2.236	2.209	3.716	3.589		3.480	3.575	2.236		3.752		1.946	3.694	3.237	3.046	3.188	3.178	3.263	2.873
H_β−C_β		1.147	1.153	1.160	1.105	1.108		1.104	1.104	1.146		1.104		1.477,1.497	1.104	1.102	1.100	1.099	1.100	1.101	1.099
IRC[h]											2.167	2.243		1.497	1.858			1.522		1.444	
∠ϕ	77	77	77	77	79	78	73	75	76	77	70	70	74	68	65	58	66	62	56	45	81
∠Cp−Nb−Bd	141	137	137	137	139	139	128	134	128	127	133	132	144	127	137	141	133	137	139	132	134

[a] The R-carbon in Figure 7. [b] The first carbon atom in the polymer chain (R is the last, see Figure 7). [c] The transferring hydrogen, i.e., the one bound to C1. [d] Hydrogen bound directly to niobium. [e] Geometry is C_s-symmetric, and both H_α atoms are equidistant from Nb. [f] Ethene carbon becoming the C_α after insertion. [g] The ethene carbon becoming C_β. [h] The length of the new bond at the transition state. [i] The methyl carbon of former butadiene. [j] Bold alphanumerics refer to structures used in figures. Property section refers to atom labels in Figure 4. The shortest Nb−H distances of the two or three possibilities are tabulated. Distances in angströms, angles in degrees

ular dynamics simulation the terminal methyl group of the propyl chain was in constant rotational motion at 300 K. These features decrease the reliability of the thermochemical data calculated using the harmonic approximation.

Ethene Coordination Step. After catalyst **1** activation, the first step in the actual polymerization cycle is the coordination of ethene to the alkyl complex **2a**. We found an energy minimum **3a** corresponding to approximately perpendicular ethene alignment relative to the plane between the ligand planes (see Figure 4.). This is in contrast to most isoelectronic cationic group IV analogues $Cp_2MR(C_2H_4)^+$, where M = Zr, Ti, Hf and R = alkyl[4,8,11,29] and $Cp_2Nb(C_2H_5)(C_2H_4)^+$ [67] where the η^2-ethene lies in a plane between the Cp ligands. Few cases have been reported where ethene coordinates also in a perpendicular fashion.[5,9,30]

Complex **3a** lies 1.0 kcal/mol lower in energy compared to the separated ethene and complex **2**. The loss of rotational and translational degrees of freedom makes the coordination Gibbs free energy high: $\Delta G = 13.7$ kcal/mol. Three local minima, confirmed by frequency calculations, were determined for the ethyl η^2-ethene complexes: two α-agostic complexes, **3b-alpha1**, 3.6 kcal/mol ($\Delta G = 16.6$), and **3b-alpha2**, 4.2 kcal/mol ($\Delta G = 18.1$), and one β-agostic, **3b-beta**, 4.3 kcal/mol ($\Delta G = 19.0$), above free ethene and **2b-beta**. The alternative, so-called backside or anti β-agostic conformation, corresponding to 180° rotation of the C_α−Nb bond, was unstable. The α-agostic geometries differ in the alkyl group orientation and therefore in the H_α participating in the agostic bond. **3b-alpha1**, the one with the lower energy, has the correct orientation for the ethene insertion, so that the agostic bond is preserved.

The energy barrier for conversion back to an alkyl complex and free ethene was estimated by calculating geometries with constrained C_{ethene}−Nb distances. The energy profile is presented in Figure 5. The figure shows that a shallow energy minimum exists, but the free energy increases monotonically upon coordination.

These η^2-ethene structures are problematic for DFT. Repeating the geometry optimization of **3a** with (B3LYP/B1), (BLYP/SDD[71]), and (BLYP/B3) resulted in ethene ejection. The ethene complex was stable and essentially similar with respect to energy and geometry using (BP86/B1), (BP86/B2), (BLYP/B2), (BLYP/DNP), and (MP2/B1). A BLYP Car−Parrinello molecular dynamics simulation of **3a** ejected ethene after a few molecular vibrations even at low temperature (100 K); while using the BP86 functional, ethene remained coordinated in either β-agostic or α-agostic conformation depending on the starting structure at 300 K. Average bond lengths calculated from the 750 fs **2b-beta** simulation were generally similar to the static Gaussian98 results: H_β−Nb 2.13, C_{up}−Nb 2.64, C_{down}−Nb 2.78, and C_α−Nb 2.30 Å. The 2 ps simulation of **3b-alpha2** at 300 K gave the following average bond lengths: H_α−Nb 2.55 (2.81 for the other H_α), C_{up}−Nb 2.46, C_{down}−Nb 2.64, and C_α−Nb 2.27 Å, where the H_α−Nb bond is markedly longer relative to the G98 static value: 2.25 Å (see Table 4 for notation and G98 values). The preliminary Car−

(71) Stuttgart/Dresden basis set and relativistic effective core potential for Nb and Dunning/Huzinaga full double-ζ for C and H. SDD keyword in Gaussian98.

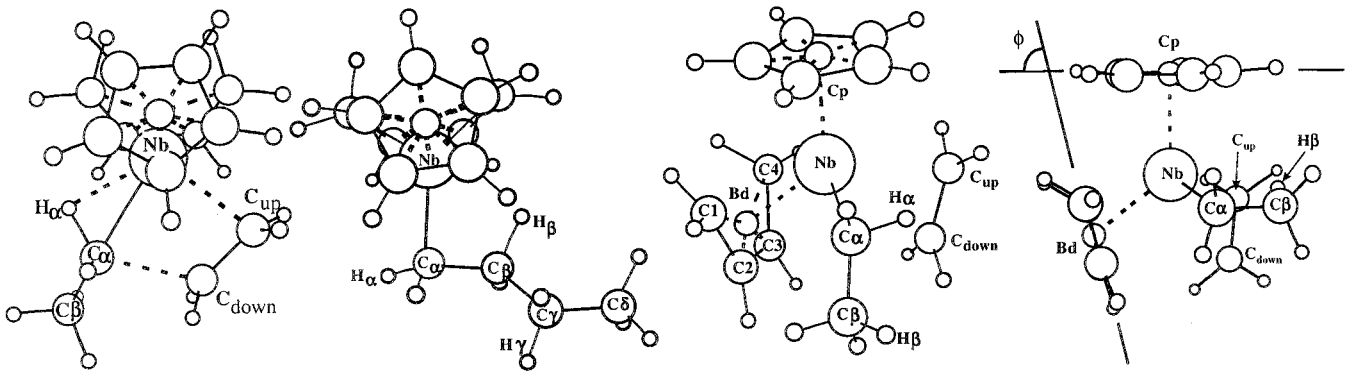

Figure 4. Example geometries to illustrate the atom labeling for geometrical data in Table 3. The geometries from the left are **[4b], 2d-beta**, **3b-alpha2**, and **3b-beta**.

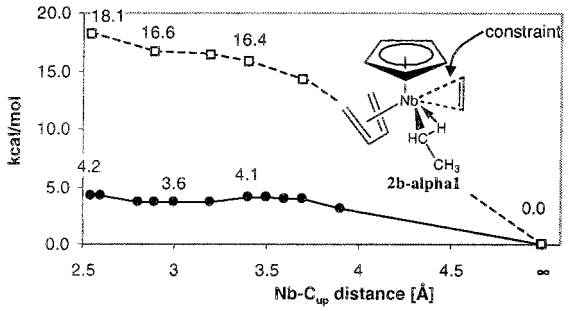

Figure 5. Energy profiles for η^2-ethene ejection (and insertion) to ethyl alkyl complex. Dotted and continuous lines depict free energy and electronic energy difference, respectively, relative to separated ethene and **2b-beta** plotted against (constrained C_{ethene})−Nb distance.

Parrinello calculations gave an ejection barrier of 3 kcal/mol, which is slightly larger than the static values. According to the ab initio calculations, the ethene coordination was stronger, and these results will be discussed at the end of the paper. These results underline the difficulty of modeling the weakly coordinating η^2-ethene complex where the dynamical correlation is important. The BP86 functional predicts endothermic η^2-ethene complexes, while BLYP and B3LYP seem to disfavor complexation.

Ethene binding in the ethyl precursor complex is less effective compared to the methyl complex, as can be seen from higher energies and longer metal−ethene bonds (see Tables 3 and 4.) The agostic interactions partially compensate the steric repulsion arising from the polymer chain, which is reflected by the different ethyl η^2-ethene complex geometries. A closer ethene approach can be achieved at the expense of the agostic bond, the former being energetically more favorable. Also, the Cp ring is differently oriented with respect to the ligands. The essential result is that the complexation is weak, and the ethene is mobile.

The ethene π-orbital has a small overlap with the metal d-orbitals at HOMO-5 and HOMO-6 binding the monomer. The π^*-orbital of ethene, which would be ideal for back-donation from the metal, is empty at the LUMO+1. One might have expected a covalent bond here, resulting in high complexation energy, according to the tendency of formally d-populated metals. Instead, the HOMO has a large contribution of the butadiene π^*-orbital and Nb d-orbitals. As Margl et al.[14] have pointed out, this is the key factor also preventing the metal lone pairs from occupying the ethene-C_α antibonding orbital at the insertion transition state and thereby increasing the insertion barrier. At the insertion transition state the antibonding orbitals with respect to the forming bond are found above the LUMO. Apart from the HOMO and the Nb(d_{yz})−Cp(π_h)−butadiene(π_h) MO at the HOMO-3 the four next occupied orbitals have bonding character either between the forming bond or with the metal. The lack of strong bonding is the difference between the studied Nb catalyst with respect to V, Cr, and Mn 1−3 d-electron catalysts, which all possess a nonnegligible (≈10 kcal/mol)[72] insertion barrier from the η^2-ethene complex. In that case the barrier is derived from the distortion of the bonding ethene π^*-metal d_{xy} interaction at the insertion transition state.

We anticipated that the low π-bonding capability would also impede toluene coordination to the metal center. Solvent coordination was investigated by trying to optimize geometries, where a toluene molecule would bind to the alkyl resting state. Optimizations were started from geometries where a toluene ring C−C bond was in the place of ethene in the template complex **3a**. The methyl complex imposes the least steric congestion around the metal and, as a first estimate, would be the easiest of the different alkyl−toluene complexes to optimize. The actual polymer chain would hinder toluene coordination even more. Two starting geometries were tested, where the toluene methyl group was pointing in opposite directions. At first, to accommodate the large toluene molecule by rearranging the rest of the complex, the closest toluene carbon atom distance to niobium was constrained. Releasing the constraint after relaxation of other degrees of freedom resulted in the ejection of the toluene molecule. This suggests that toluene does not bind to the metal catalyst, as has been reported for the zirconium analogues.[4,7] We propose this as a feature to compensate for the low complexation efficiency caused by the weak coordination of ethene relative to analogous zirconium catalysts.

Insertion Step. There are several alternatives after ethene complexation: ethene ejection, ethene insertion to the metal−alkyl bond, and hydrogen transfer between the alkyl and ethene moieties. To proceed in the catalytic cycle, we will discuss the 1,2-migratory insertion pathway from the η^2-ethene complex intermediate.

The 1,2-ethene insertion can, in principle, start from any alkyl conformation. In the first cycle β-agostic

(72) Schmid, R.; Ziegler, T. *Organometallics* **2000**, *19*, 2756−2765.

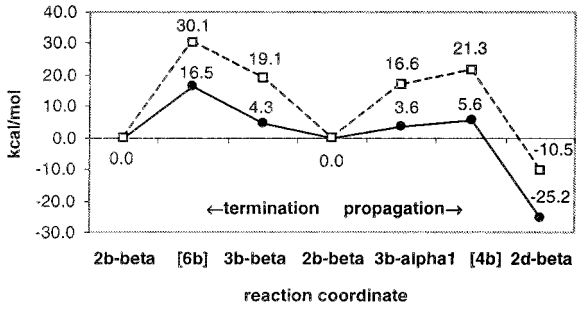

Figure 6. Concerted complexation and insertion steps (to the right), when the polymer is modeled with an ethyl moiety, and termination via β-hydrogen exchange to the left from the same precursor. Dotted and continuous lines depict free energy and electronic energy difference, respectively, relative to separated ethene and **2b-beta**.

interaction is not possible due to lack of β-hydrogens. When the growing polymer was modeled with an ethyl group, the insertion potential energy scan was started from the lowest free energy α-agostic conformer, **3b-alpha1**, to the transition state **[4b]**. In the transition state **[4a]** the C_α,C_β, and C_γ atoms are nearly in a plane perpendicular to the butadiene(center)−Nb−Cp(center) plane. The transition state is clearly stabilized by agostic interaction. The agostic H_α−Nb bonds are 2.16 and 2.07 Å in **[4a]** and **[4b]**, respectively. The first insertion barrier (the alkyl site is occupied by a methyl group) from **3a** via **[4a]** to **2c-beta** was calculated to be 4.5 ($\Delta G^\ddagger = 7.0$) kcal/mol. The geometrical data are presented in Table 4 and energies in Table 3, and the insertion profile is shown in Figure 6.

The ethene coordination reaction step to the ethyl complex **2b-beta** → **3b-alpha1** was calculated to be endothermic by 3.6 kcal/mol, and the insertion barrier **3b-alpha** → **[4b]** → **2d-beta** was calculated to be only 1.9 kcal/mol. Ethene insertion led directly to a β-agostic conformation with both modeled starting complexes.

The electronic barriers after ethene coordination are comparable to the Zr and Ti analogues. The high free energies of ethene complexation reflect the lower catalyst activity of niobium. The experimental activity of the **1** + MAO catalytic system is low, for example, compared to Cp_2ZrCl_2 + MAO (3.9×10^4 kg/h·mol·[Zr]·atm, T = 343 K, $p(C_2H_4) = 1.5$ atm).[73] The experimental activity for the Cp(2,3-dimethylbutadiene)$NbCl_2$ + MAO catalytic system is 6.89 kg/h·mol·[Nb] ($p(C_2H_4) = 1$ atm, T = 293 K), and for Cp*(butadiene)$NbCl_2$ + MAO 10.65 kg/h·mol·[Nb] ($p(C_2H_4) = 1$ atm, $T = 253$ K). The former catalyst produced polyethylene with low monodispersity and the latter with 1.05 (M_w/M_n) and exhibited living polymerization characteristics.[18]

The energy profile for propagation is essentially the same when the alkyl part is modeled with a methyl and an ethyl group. The ethene complexation is only slightly stronger in the methyl case, due to the less crowded metal center, but the free energies are close to each other. The transition state structures **[4a]** and **[4b]** with methyl and ethyl groups as the growing polymer chain, respectively, are practically similar (see Table 4). The rate-determining step based on our calculations is the very weak ethene coordination together with the insertion in a concerted fashion.

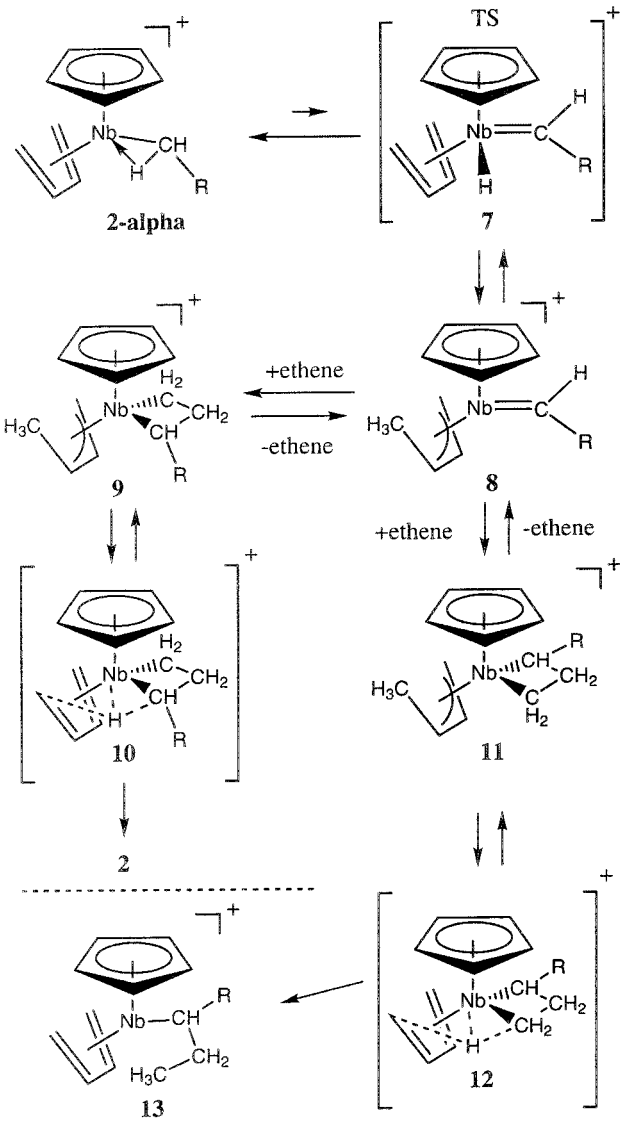

Figure 7. Alkylidene formation from the α-agostic alkyl complex and possible further reactions with ethene. Alphanumerics as in Figure 2.

The insertion transition states exhibit the strongest agostic bonding detected in this study. It can be verified by the low CH-stretching frequencies, elongated CH bonds, small Nb−C_α−H_α angles, and close H−Nb distances.[65] The H−Nb distances are not quite as small as reported in analogous Zr or Ti complexes. However, the shift in the calculated CH-stretching frequencies provides evidence for the weakening of the H−C bond and strengthening of the H−Nb bond. The symmetric CH_3 stretching is the lowest CH frequency in **2a** (2865 cm^{-1}). The agostic hydrogen stretching frequencies were calculated to be 2610, 2543, and 2486 cm^{-1} in **2b**,**c**,**d-beta**, respectively, and 2643 and 2506 cm^{-1} in **[4a]** and **[4b]**, respectively.

Alkylidene Formation. As an alternative reaction path corresponding to mechanism 2, the formation of an alkylidene intermediate from the alkyl complexes was calculated (see Figure 7). The energy profile for conversion of **2b-alpha2** to an alkylidene hydride was scanned by increasing the C_α−H_α bond length. No stable

(73) Chien, A. C.; Ravazi, A. *J. Polym. Sci. Part. A: Polym Chem.* **1988**, *26*, 2369.

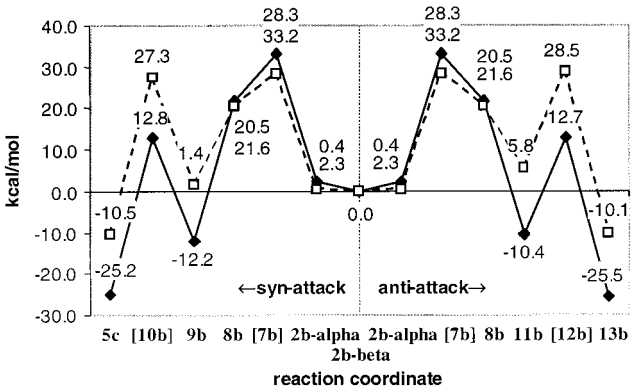

Figure 8. Alkylidene formation and subsequent ethene insertion leading to metallacycles. The coordination of incoming ethene syn to the methyl group of the methyl allyl moiety is presented to the left. Dotted and continuous lines depict free energy and electronic energy difference, respectively, relative to separated ethene and **2b-beta**. The upper values in the graph refer to the free energies.

hydride but a transition state **[7b]** was found at a $C_\alpha-H_\alpha$ distance of 2.362 Å, 33.2 ($\Delta G = 28.3$) kcal/mol above **2b-beta** (see Figure 8). Extending the scan beyond the hydride-TS led eventually to coordination of the former α-hydrogen to the terminal butadiene carbon, producing an ethylidene complex **8b**, 21.6 ($\Delta G = 20.5$) kcal/mol above **2b-beta**. The butadiene ligand is able to accommodate the hydrogen atom while adopting π-allyl coordination to the metal. This intermediate does not strictly speaking conform to the Green−Rooney mechanism, but could be thought of as a modification of it. The allyl complex might undergo several different reactions. However, in this paper we investigate only the ethene uptake necessary for polymerization to proceed.

While trying to optimize η^2-ethene complexes of **8b**, ethene adds directly to the carbene bond, forming the metallacycles *syn*-**9d** and *anti*-**11d**, depending on the original position of ethene relative to the methyl−allyl moiety. This is not surprising considering the high reactivity of metal carbenes and the more exposed metal surface relative to (β-agostic) alkyl complexes. The energy barrier from alkyl to the alkylidene complex is well above the presented propagation step, but in the range of termination steps. One of the methyl hydrogens in methyl−allyl moiety is at 2.402 Å ($r_{CH} = 1.128$ Å) distance from the metal. This already corresponds to a weak agostic interaction. The energies of the isomers are practically equal, −9.9 ($\Delta G = 6.2$) and −10.4 ($\Delta G = 5.8$) kcal/mol for **9d** and **11d**, respectively, relative to separated **8b** and ethene. Hydrogen migration from methyl−allyl through TS **[10d]** and **[12d]** have activation barriers of 24.9 ($\Delta G^\ddagger = 26.0$) from *syn*-**9d** and 23.1 ($\Delta G^\ddagger = 22.7$) kcal/mol from *anti*-**11d**. The hydrogen is stabilized by the metal during transfer between the metallacycle and methyl−allyl moieties. According to the small difference in the previous barriers, there should be no preference for the linear polymer via this route.

The continuation of polymerization requires new monomer incorporation, but the ethene coordination to the 2-butyl alkyl complex should be extremely difficult due to steric repulsion at the metal center, suggesting that the polymerization does not proceed via this route.

Mashima et al. have also detected a niobium alkylidene species derived from a similar niobocene compound.[57] We calculated the dimethyl starting complex ($Cp(butadiene)Nb(CH_3)_2$), which might also result from methylation of both halogens in **1** and found it to be metastable by −1.0 ($\Delta G = -12.3$) kcal/mol with respect to decomposition into methane and a methylidene complex. The transition state resembles the resulting methylidene complex and lies 24.3 ($\Delta G^\ddagger = 24.0$) kcal/mol above the dimethyl complex. The breaking CH bond at the transition state is 1.52 Å, the forming methane CH bond 1.47 Å, and the Nb−H bond 1.89 Å. The exergonic decomposition is in agreement with experimental thermal instability, as reported by Mashima et al. This complex has also been reported to catalyze ROMP. However, the methylidene complex is neutral, does not have the necessary hydride, and therefore does not conform to reaction mechanism 2. The complexes **9** and **11**, on the other hand, could be thought of as ligand-assisted Green−Rooney mechanism intermediates.

Termination Step. The principal polymerization termination mechanisms are via β-hydrogen transfer either (i) to coordinated alkene or (ii) to the metal. The former produces an alkyl complex and the latter a metal hydride after alkene ejection.[1,4,7,13,74] Hydrides for niobocenes are known.[67,75] Polymerization may be also quenched by adding dihydrogen. In this case a metal hydride and a saturated alkane are formed. This mechanism is not considered here, since we are interested in the competing processes in propagation conditions.

The termination by β-hydrogen transfer to coordinated ethene is presented in Figure 6. We started the TS optimization from a complex where the breaking and forming CH bonds were forced to be of equal length. Then this constraint was scanned for a minimum, thus presupposing a C_s-symmetric transition state with respect to the CH bonds. An unconstrained TS search based on second derivatives from this minimum resulted in an almost C_s-symmetric transition state with an energy of 16.5 (18.6 with CCSD/B1//BP86) kcal/mol above separated reactants and 12.2 kcal/mol above **3b-beta**. The corresponding $\Delta G^\ddagger$ values are 30.1 and 11.0 kcal/mol, respectively. The ethyl carbon atoms, the transferring hydrogen, and the metal center were in a plane between the ligand planes. The frequency calculation revealed a single imaginary mode corresponding to a highly localized hydrogen movement between neighboring carbon atoms participating in the reaction step, and a series of eigenmode following calculations along the imaginary mode connected the reactant and product complexes. Further proof for the TS and reaction path is given by a constrained Car−Parrinello molecular dynamics run on the same reaction. It was driven by gradually decreasing the ethene carbon−H_β distance, producing an essentially similar, almost C_s-symmetric, transition state. The newly formed ethene molecule ejected immediately from the complex after the TS.

The alternative β-elimination termination mechanism starts from the alkyl complex (see Figure 2). Previously,

(74) Deng, L.; Margl, P.; Ziegler, T. *J. Am. Chem. Soc.* **1997**, *119*, 1094−1100.
(75) Burger, B. J.; Santarsiero, B. D.; Trimmer, M. S.; Bercaw, J. B. *J. Am. Chem. Soc.* **1988**, *110*, 3134−3146.

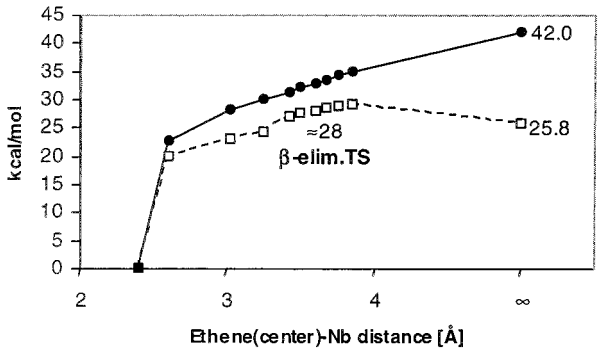

Figure 9. Energy profiles for β-elimination of the propyl chain starting from **2c-beta** producing **5** and free propene. The energy profile is plotted against Nb−propene double bond center distance. Dotted and continuous lines depict free energy and electronic energy difference, respectively, relative to **2c-beta**. The free energy barrier at 3.5 Å is 28 kcal/mol; see text for discussion.

it has been shown that modeling the polymer with an ethyl group overestimates the termination barrier, and thus we used a propyl group (although the termination product energy difference is not a straightforward function of the polymer length, see Table 3).[76] Increasing the agostic $C_\beta-H_\beta$ bond to determine the potential energy profile for hydrogen transfer to metal led to a structure reminiscent of a metal hydride and η^2-coordinated alkene at a $C_\beta-H_\beta$ separation around 2.7 Å. The potential energy scan profile had a plateau at 2.5−2.9 Å, but no energy minimum was found, and the force on the constraint was monotonically negative. The electronic and free energies at constraint value 2.7 Å were 22.7 and 20.0 kcal/mol above **2c-beta**, respectively. When separated from the H_β, the propyl group adopts a perpendicular orientation of the double bond relative to the plane between the ligand planes. To effect the alkene dissociation from the metal, we scanned the former $C_\beta-Nb$ distance starting from the hydride-like structure with a constraint value of 2.8 Å. The termination energy profile is presented in Figure 9. The potential energy increases monotonically with distance, but there might be a maximum on the calculated free energies at some distance. We used large constraint values as the $C_\alpha-Nb$ distance remained short and roughly corresponded to $C_{ethene}-Nb$ bonding distances in η^2-complexes in the calculated structures. Coordination via C_α reduced the propene's rotational and translational freedom, resulting in a small free energy barrier. At long distances the propene becomes very loosely bound and the determination of entropies becomes unreliable. Also, in the real conditions the ejecting alkene is already interacting with the solvent, and the gas phase results become irrelevant. We approximate the gas phase elimination free energy barrier $\Delta G^{\ddagger} \approx$ 28 kcal/mol at the double bond−Nb distance 3.5 Å ($C_\alpha-Nb$ distance 3.1 Å), where the energy change essentially levels off. This is very close to the infinite separation energy difference and even closer to the free butene + **5** energy.

A Car−Parrinello constrained dynamic simulation followed a qualitatively similar pathway with a plateau after the breakage of the $C_\beta-H_\beta$ bond and before dissociation of the alkene without detectable minimum energy intermediates. Also in this case the C_α remained coordinated to the metal.

Discussion

The highest level of theory used in this study, the CCSD method, locates the insertion transition state **[4b]** 3.4 kcal/mol above separated products and predicts the β-elimination products to be 54 kcal/mol above the starting alkyl complex, which is well above the insertion barrier. In general it can be seen that both CCSD and MP2 give higher binding energies to the alkyl and alkenyl groups. Even after correcting for BSSE the MP2 binding energies are 3−9 kcal/mol higher than with DFT. It is perhaps not safe to use the difference **2b-beta** → (**5** + ethene) ΔE(CCSD/B3−CCSD/B1) to correct for the basis set improvement for all intermediates, but the same trend is seen also in the diimine ethene complexation energies in Table 1. The complexation energies on the diimine system with BP86 and CCSD are in better agreement than in the case of niobium metallocene complexes. This might be due to the approximate way in which DFT describes electron correlation and leads to the different recovery of the correlation energy in different systems. To find out the upper and lower bounds for the energetics, we will account for the unrecovered correlation energy (which still is very likely a lower bound for CCSD due to the modest basis set) by taking the CCSD energies and calculating the corresponding free energies using the thermodynamical data extracted from BP86 frequency calculations. The free energy barrier for propagation can be estimated by correcting the CCSD value by the BP86/B1 free energies: adding $\Delta\Delta = (\Delta G$**[4a]** $- \Delta E$**[4a]**) to the CCSD insertion barrier, yielding $\Delta G^{\ddagger} \approx 3.4 + (21.3 - 5.6) \approx 19$ kcal/mol. The β-hydrogen transfer barrier can be approximated in a similar fashion to be $\Delta G^{\ddagger} \approx 18.6 + (30.1 - 16.5) \approx 32$ kcal/mol and β-elimination products $\Delta G \approx 53.6 - (45.6 - 29.6) \approx 38$ kcal/mol. The β-elimination free energy barrier can be approximated in the following way: the difference from the BP86 calculations between (ΔG**[5** + propene**]** $- \Delta G^{\ddagger}$**[**β**-elim. TS]**) = $\Delta\Delta$ (to account for the effect of binding to the metal before the translational and rotational degrees of freedom are fully populated) is added to the termination product (estimated) free energy calculated with CCSD/B3, yielding $\Delta G^{\ddagger} \approx 38 + (28.0 - 25.8) \approx 40$ kcal/mol. The approximated barriers thus prefer propagation over hydrogen transfer by 13 kcal/mol. By making some more approximations we can look at the effect of these energies on the polymerization dynamics. If we take the preexponential factors of the Eyring equation as equal and assume steady state conditions for the η^2-ethene complexes, there should be $\approx 10^9$ insertions to one termination. This agrees with the experimental results where long polymers with analogous complexes were obtained. However, one should be careful in applying vacuum results of the model system to condensed phase reactions.

The transfer of the alkyl$-H_\alpha$ to the butadiene ligand was an unexpected reaction path revealed by the CPMD simulations. The propagation of polymerization via this is nevertheless unlikely: the ethene coordination is

(76) Woo, T. K.; Margl, P. M.; Ziegler, T.; Blochl, P. E. *Organometallics* **1997**, *16*, 3454−3468.

already the dynamical bottleneck in the terminal alkyl complexes and the polymer coordination via the 2-carbon would block the metal from the monomer even more in the next insertion step. This might still be an important mechanism inducing polydispersity by deactivation through hindered reactivity or by causing some other side reactions.

On the basis of these energy barriers we suggest the prevailing mechanisms to be propagation and β-hydrogen transfer to coordinated monomer. The uncertainty in the ethene coordination does not affect their relative probablities. Also the reactant concentration dependencies are equivalent, as would not be the case if the unimolecular β-elimination were more facile. The 8 kcal/mol (derived from CCSD energies above) activation free energy difference in favor of the β-hydrogen transfer to coordinated monomer relative to β-elimination makes it intrinsically (the Boltzman factor) 6 orders of magnitude more likely. The energy differences of these termination steps were negligible by the self-consistent BP86/B1 approach, thus favoring the unimolecular β-elimination. The differences in the complexation energies between various methods decrease their reliability, and the model may be too simple to account for the delicate features shaping the polymer size distribution: basically any of the presented possible termination mechanisms (including alkylidene formation) may be operative, and their relative importance would be decided by the substituents, temperature, counterion, or solvent. Computational studies on ligand effects and differences between Nb and Ta as the metal center on the model system described in this paper are in progress.

Conclusions

We have calculated, using DFT, the primary steps of the model niobocene polymerization catalyst and compared the key step results to correlated ab initio calculations. Our results suggest a mechanism where the α-agostic interaction is crucial only in the insertion transition state and where the insertion is concerted-like.

The studied catalyst differs from Cp_2ZrR^+, and analogous group III,IV d^0-complexes, in two major ways: Typically, there exists a stable ethene complex before the insertion step. However, in this case the rate-determining step (RDS) is clearly the combined coordination and insertion step without detectable free energy minima (DFT) between, as the ethene coordination to the alkyl complex is very weak. Second the strong agostic interaction in the resting state alkyl complex is lacking in contrast to group III neutral and group IV cationic isoelectronic analogues.

The largest differences between various computational methods appear in the active site binding energies. MP2 and CCSD predict higher complexation energies than DFT. The high MP2 complexation energies are reduced almost to the same level with DFT after correcting for BSSE, which is 12−17 kcal/mol larger for MP2. The intramolecular energy barriers on the other hand are in fair agreement. The weak DFT complexation, relative to MP2 and CCSD, probably should be corrected to decrease the RDS barrier and the possibility of β-elimination. DFT still appears as an economic method, with a small BSSE, to thoroughly explore the potential energy surface without the unwieldy counterpoise method.

It is interesting to note that an effective catalyst need not have strong η^2-alkene coordination capability, although this is reflected in the lower activity, but on the other hand results in high molecular weights and in certain cases monodisperse polymer. All levels of theory resulted in positive free energies of complexation. The BSSE-corrected propagation energy barriers after ethene coordination are small ($\Delta E^{\ddagger} = 1.3-3.5$ kcal/mol) with all theories (5.7 with CCSD). However, as the complexation is endothermic, the true barrier should be calculated relative to separated reactants. In that case the conversion of rotational and translational degrees of freedom to vibrations upon coordination increases the insertion free energy barrier by approximately 16 kcal/mol, resulting in much higher barriers: $\Delta G^{\ddagger} = 19-24$ kcal/mol (BLYP and HF excluded). The insertion barrier consists mostly, roughly by 80%, of the coordination of ethene.

The barrier for hydrogen transfer between the polymer and monomer, leading to terminal alkene ejection and termination, was calculated to be 16−19 ($\Delta G^{\ddagger} = 30-32$) kcal/mol, relative to separated reactants. This reaction channel is unlikely due to the high activation energy. H_β-elimination, followed by alkene ejection without stable intermediates, was also expensive: $\Delta E = 40-49$ kcal/mol (BLYP and HF excluded) for the products and $\Delta G^{\ddagger} = 28$ kcal/mol (BP86) for the barrier.

The most important free energy barriers calculated using CCSD energies corrected by entropies from BP86 calculations give the following values: 19 kcal/mol for propagation, 32 kcal/mol for β-hydrogen transfer to coordinated monomer, and 40 kcal/mol for β-hydrogen elimination. Apart from the latter the results are in good agreement with the BP86 results. The first two are likely to be upper bounds, as the modest DZ-quality basis will not be able to recover a sizable amount of the correlation energy. On the whole one can say that this niobium metallocene complex is a demanding system to model theoretically, and it is reasonable to compare the results between different methods.

For catalysis to take place, first a free coordination site for the incoming alkene must be available. In our case the high propagation barrier may be compensated by the availability of the reactive site as the π-type complexation capability is weak and also solvent coordination on the active site, which has been suggested as a factor to diminish catalytic activity on Cp_2ZrR^+, is small.

Acknowledgment. The authors gratefully thank the Magnus Ehrnrooth Foundation, The Helsinki Institute of Physics, and the Academy of Finland for financial support. The Center of Scientific Computing is especially acknowledged for professional support and most importantly for providing both the hardware and software at our disposal to perform the computations.

OM0010924